Title

Ground-Motion Model for Significant Duration Constrained by Seismological Simulations

Authors

Pinilla-Ramos, Camilo

Abrahamson, Norman

Phung, Van-Bang

et al.

Publication Date

2023-12-06

DOI

10.1785/0120230139

Peer reviewed

Ground-Motion Model for Significant Duration Constrained by Seismological Simulations

Camilo Pinilla-Ramos*[1], Norman Abrahamson[1], Van-Bang Phung[1], Robert Kayen[1], and Pablo Castellanos-Nash[2]

ABSTRACT

A duration ground-motion model for crustal earthquakes based on the normalized Arias intensity (I_A) is developed. Two sets of seismological simulations are used to constrain the form and scaling of the duration model. Simulations using a 3D crustal model show that an additive model for the source, path, and site terms captures the physical behavior of duration better than a multiplicative model for the site term. Stochastic finite-fault simulations are used to constrain the saturation of the large-magnitude scaling at short distances. The duration model is developed in two parts: a duration model for the time interval between 5% and 75% of the normalized Arias intensity (D_{5-75}) and a duration model for the ratio of the D_{5-X}/D_{5-75} duration for X values from 10 to 95. Together, these two models provide a more complete description of the evolution of the seismic energy with time than a single duration metric. A new aspect of the statistical model for duration is the inclusion of a random effect for the path term in addition to random effects for the source and site terms. The source and site random effects are modeled as scale factors on the duration, whereas the path-term random effect is a scale factor on the distance slope. The distribution of the duration residuals has a skewness that is between the skewness of a lognormal distribution and the symmetry of a normal distribution. The final duration aleatory variability is modeled by a power-normal distribution with an exponent of 0.3, which accounts for the amplitude dependence of the aleatory variability of the duration with smaller aleatory variability for large-magnitude events and larger aleatory variability for small-magnitude events as compared to the variability from a lognormal distribution.

KEY POINTS

- Recent empirical duration models do not have a proper physical basis, so they do not extrapolate properly.
- The duration follows an additive form with short-distance saturation and follows a power-normal distribution.
- The methodology for combining numerical simulations and empirical data can be applied to other topics.

Supplemental Material

INTRODUCTION

Many earthquake engineering applications require an estimate of the ground-motion duration in addition to an estimate of the amplitude. For example, ground-motion duration is a key parameter in geotechnical engineering applications involving nonlinear deformation regimes, such as liquefaction analysis or large deformation numerical modeling (Seed, 1975; Bray and Travasarou, 2007; Idriss and Boulanger, 2008; Bray and Olaya, 2022). Duration is also required for applications of random vibration theory to estimate the peak amplitudes in the time domain from a Fourier amplitude spectrum (Rathje and Kottke, 2008).

The most commonly used definition of duration is based on the normalized Arias intensity (I_{AN}; Arias, 1970) given by

$$I_{AN}(t) = \frac{\int_0^t a(\tau)^2 d\tau}{\int_0^{t_{max}} a(\tau)^2 d\tau}, \quad (1)$$

in which $a(\tau)$ is the acceleration time series. Equation (1) can be inverted to give the time as a function of the I_{AN}. The duration is defined as the time between the $I_{AN}(t)$ reaching two selected percentages X and Y:

$$D_{X-Y} = t(I_{AN} = Y) - t(I_{AN} = X), \quad (2)$$

1. Department of Civil Engineering, University of California, Berkeley, California, U.S.A., https://orcid.org/0000-0002-4034-6618 (CP-R); https://orcid.org/0000-0001-7900-6023 (NA); https://orcid.org/0000-0002-3269-7792 (V-BP); https://orcid.org/0000-0002-0356-072X (RK); 2. CDS, Universidad de Concepción, Concepción, Chile, https://orcid.org/0000-0002-8585-8035 (PC-N)

*Corresponding author: camilo.pinilla@berkeley.edu

Cite this article as Pinilla-Ramos, C., N. Abrahamson, V.-B. Phung, R. Kayen, and P. Castellanos-Nash (2023). Ground-Motion Model for Significant Duration Constrained by Seismological Simulations, *Bull. Seismol. Soc. Am.* **XX**, 1–18, doi: 10.1785/0120230139

in which $t(I_{AN} = X)$ is the time at which the normalized Arias intensity equals to X.

The duration can be partitioned into the source, path, and site terms. The source term is due to the duration of the finite-rupture process and controls the duration at short distances on hard-rock site conditions. The path term represents the increase in the duration due to wave reflection, refraction, and scattering in the deep portion of the crust and due to the dispersive nature of surface waves. The site term represents the increase in the duration due to reflection, refraction, and wave scattering in the shallow 3D velocity structure at the site.

In the recent decades, several empirical models for duration have been developed (e.g., Herrmann, 1985; Silva *et al.*, 1996; Kempton, 2006; Bora *et al.*, 2014; Boore and Thompson, 2014; Afshari and Stewart, 2016; Bahrampouri *et al.*, 2021; Bommer *et al.*, 2021). Most models have assumed that the aleatory variability of the duration is log-normally distributed, but they have used different assumptions for how the source, path, and site effects are combined: additive forms, multiplicative forms, or a combination of both additive and multiplicative forms.

The additive form is based on the seismological concept in which the source is divided into subevents, and the waves are propagated from each subevent to the site. At the site, the ground motion is the sum of the waveforms from each subevent. The waveform from each subevent includes the path effects. The time shift between the waveforms from different subevents is due to the time delays between the subevent ruptures and the differences in travel time due to different distances from the site to the subevents. With this simple physical model, the duration of the ground motion at the site is the sum of the source duration and the path duration:

$$\mathrm{Dur} = f_{\mathrm{source}}(\mathbf{M}) + f_{\mathrm{path}}(R). \quad (3)$$

This form of duration, without a site term, is commonly used in the point-source modeling of ground motion. For example, the program SMSIM (Boore, 2009) computes the ground-motion duration using this form.

With the assumption that the duration residuals are log-normally distributed and including the site term, the model for the duration with the additive form is given by

$$\ln(\mathrm{Dur}) = \ln(f_{\mathrm{source}}(\mathbf{M}) + f_{\mathrm{path}}(R) + f_{\mathrm{site}}(V_{S30})) + \delta, \quad (4)$$

in which δ is normally distributed with mean 0 and standard deviation σ. This form was used by Silva *et al.* (1996).

Other duration models have used a multiplicative form for the source, path, and site terms (e.g., Bora *et al.*, 2014). This approach treats the duration using the same statistical modeling that is applied to ground-motion amplitudes without regard to the physical basis for the scaling of duration with magnitude and distance. In a multiplicative form, the log of the duration is the sum of the source, path, and site terms:

$$\ln(\mathrm{Dur}) = g_{\mathrm{source}}(\mathbf{M}) + g_{\mathrm{path}}(\mathbf{M},R) + g_{\mathrm{site}}(V_{S30},\mathbf{M}) + \delta. \quad (5)$$

In this form, the statistical modeling is much simpler than for the additive form, and standard regression methods used for ground-motion models (GMMs) for response spectral values (pseudospectral acceleration [PSA]) can be directly applied; however, without a physical basis for the functional form, the model has to include counter-acting nonphysical features in the scaling. For example, a strong magnitude dependence needs to be included in the path term to reduce the path scale factor for large magnitudes and increase the path scale factor for small magnitudes. It is possible to find a set of coefficients for a multiplicative model that fits the available data, but this type of purely empirical model cannot be reliably extrapolated to magnitudes and source-to-site distances outside the data range as is required in many seismic hazard applications.

Recently, Afshari and Stewart (2016) and Bahrampouri *et al.* (2021) developed duration models using a mixture of additive and multiplicative forms. In these two duration models, the source and path terms are additive, but the site term is multiplicative:

$$\ln(\mathrm{Dur}) = \ln(f_{\mathrm{source}}(\mathbf{M}) + f_{\mathrm{path}}(\mathbf{M},R)) + g_{\mathrm{site}}(V_{S30}) + \delta. \quad (6)$$

The separation of the wave propagation effects into the path and site terms is arbitrary; the Earth does not know where the path ends and the site begins; therefore, from a simple seismological basis, the duration model should be additive for both the path and site effects. The distinction between site and path is often adopted in GMMs to separate regional effects related to the path through the crust, which are in the linear range from local effects in the shallow material, which can have strong nonlinear effects.

Bahrampouri *et al.* (2021) found that, from a statistical basis, the duration data did not clearly favor either the additive or the multiplicative model form for the site term. They selected a multiplicative site term form based on comparisons of duration from surface and borehole data, which showed that the difference between the duration for soil sites at the surface and the duration for rock at the base of the borehole was not constant and increased with distance. The multiplicative site term form was selected, because it was more consistent with this distance dependence than an additive site factor.

In this study, we make several improvements to the existing duration developed. The five main new features of our duration model are summarized subsequently. First, we use 3D simulations for a simple basin structure to show that the additive form leads to a magnitude-independent site term, whereas the multiplicative form requires a magnitude-dependent site term. Second, we use stochastic finite-fault simulations to constrain the

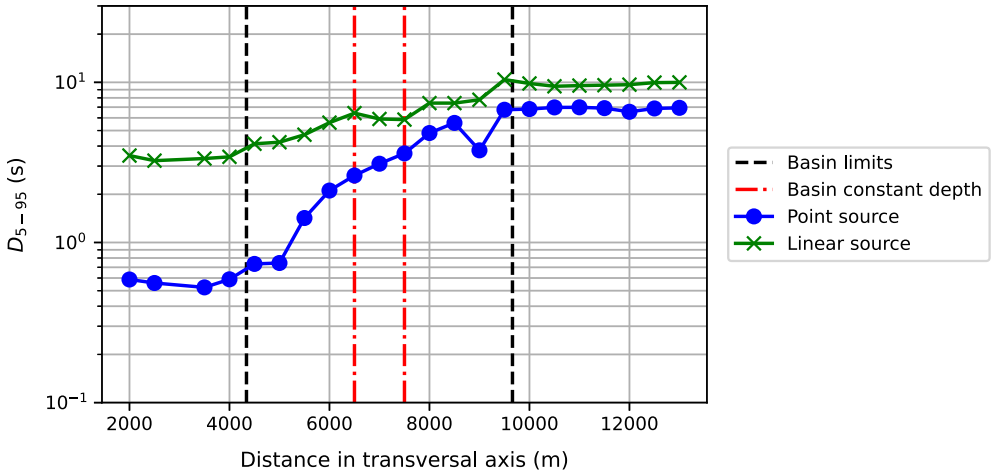

Figure 1. $D_{5–95}$ for the point-source and finite-source scenarios as function of the horizontal coordinate. The vertical dashed lines represent the basin limits. The color version of this figure is available only in the electronic edition.

saturation the large-magnitude scaling at short-distance scaling. Third, we show that the duration residuals are better modeled by a power-normal distribution than by the commonly assumed log-normal distribution. Fourth, we develop an approach for including random effects for the source, site, and path terms for an additive form of the duration model that better captures the correlation of the path effects within an earthquake. Fifth, our model includes a more complete description of the evolution of the strength of shaking with time that can be used to compute the $D_{5–X}$ duration for values of X ranging from 10 to 95.

3D SEISMOLOGICAL SIMULATIONS

To provide insights into the appropriate functional form for the site term (additive or multiplicative), we use 3D seismological simulations with a simple basin structure to compute the site effects on duration and evaluate which of the two alternative forms is more consistent with the simulation results.

The velocity model consists of a half-space with a shear-wave velocity (V_S) of 2.0 km/s. To induce strong site effects on the wavefield, we added a trapezoidal-shaped basin into the half-space (Fig. S1, available in the supplemental material to this article). The basin has the maximum depth of 0.35 km, and the edges of the basin have slopes of 16.2%. The basin material has a constant V_S of 0.6 km/s. We performed the simulations using the Seismic Wave 4 (SW4) code (Petersson and Sjögreen, 2012, 2015; Sjögreen and Petersson, 2012). Details of the 3D velocity model, the source model, and the simulation mesh are given in the supplemental material.

We performed the analysis for two seismic sources. The first case is a point-source, and the second case is a linear source with 8 km length, modeled by nine point sources spaced at 1 km intervals (Fig. S1). The point sources rupture sequentially every 0.588 s to simulate an advancing rupture front at fixed rupture velocity of 1.7 km/s from one edge of the rupture.

3D simulation results

The basin material is uniform; however, there is significant variability in both the ground-motion amplitude and the duration at sites located in the basin (Figs. S2, S3). To emphasize the effects of the site on the duration for our evaluation of the functional form for the site term, we used the $D_{5–95}$ duration metric. The $D_{5–95}$ values for the two sources are shown as a function of horizontal distance in Figure 1. Outside the basin between coordinates 2000 and 4500, the $D_{5–95}$ has the smallest value and is relatively constant, indicating that the source controls the duration without a significant increase in duration induced by path or site effects. Inside the basin between coordinates 4500 and 9500, $D_{5–95}$ starts to grow and shows the effects of the basin structure on the duration of the ground motion. For nonbasin sites located on the far side of the basin (coordinates greater than 9500), the duration stays elevated.

For the additive site-term form, the duration model is given by

$$D_{5–95–\text{add}} = D_{\text{source}} + D_{\text{path}} + D_{\text{site}}, \tag{7}$$

and for the multiplicative site-term form, the duration model is given by

$$D_{5–95–\text{mult}} = (D_{\text{source}} + D_{\text{path}}) \times D_{\text{site}}. \tag{8}$$

We use the mean of the four receivers located between coordinates 2000 and 4000 (Fig. 1) as an estimate of the source duration. Assuming that the path term is negligible for these short distances, the site term for the additive form is given by the difference in the duration at the site and the source duration:

$$D_{\text{site–add}} = D_{\text{obs}} - D_{\text{source}}, \tag{9}$$

and the site term for the multiplicative form is given by the ratio of the duration at the site and the source duration:

$$D_{\text{site–mult}} = \frac{D_{\text{obs}}}{D_{\text{source}}}. \tag{10}$$

The duration site term is shown as a function of the horizontal coordinate for the two alternative forms in Figure 2. To be consistent with each form, the site term is plotted on a linear scale for

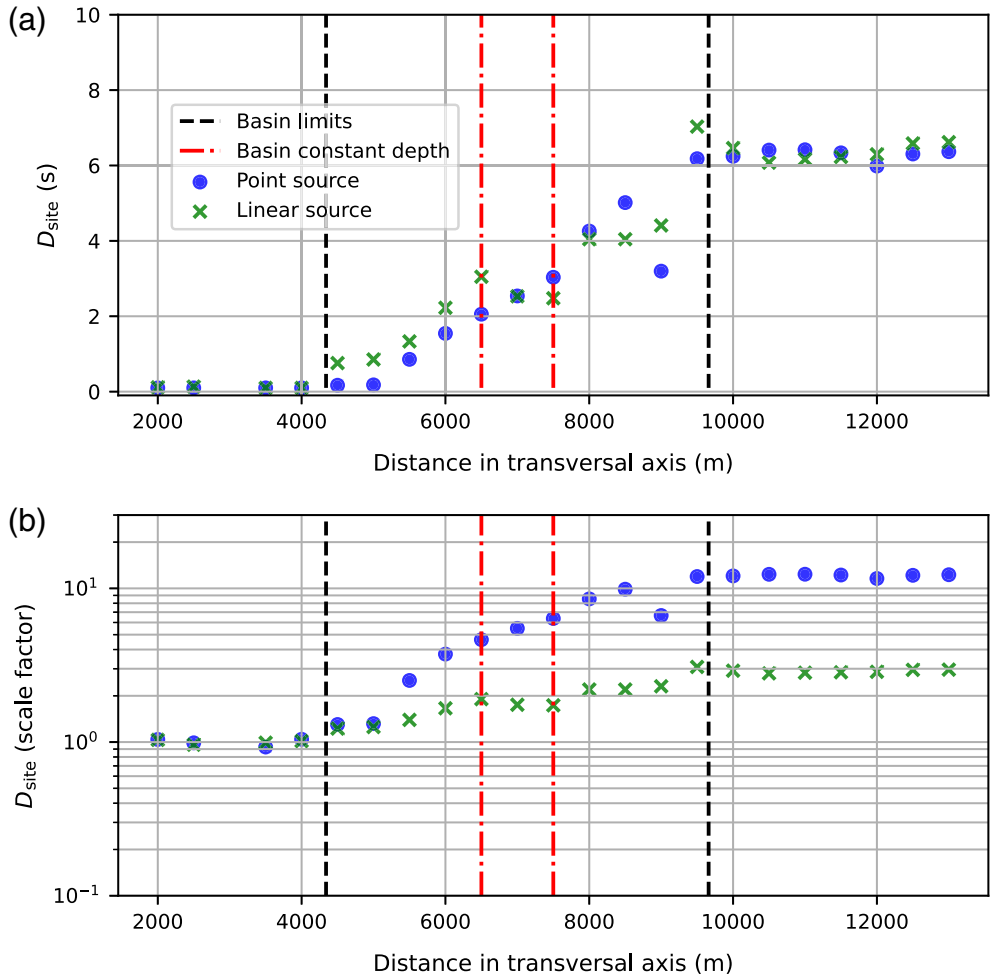

Figure 2. (a) The D_{5-95} site terms computed with the additive form. (b) The D_{5-95} site terms computed with the multiplicative form. The vertical dashed lines represent the basin limits. The color version of this figure is available only in the electronic edition.

the additive form and on a log scale for the multiplicative form. Ideally, the site term would reflect the site effects and be independent of the source given the linear constitutive model used in the simulations. Using the multiplicative approach (Fig. 2b), there is a significant difference in the site terms for the point source and finite source that represent different magnitudes. For the multiplicative form, fitting the duration data would require including a magnitude-dependent site term. In contrast, for the additive form (Fig. 2a), the site terms are similar for the two sources, leading to magnitude-independent site terms. We repeated the analysis for the D_{5-75} duration and found similar results (Fig. S4).

Based on these simulation results, we conclude that the duration values from the 3D simulation are more consistent with an additive form than with the multiplicative form for the site term for short distances. Although empirical equations can capture the site effects on duration using either form, the physical basis for the additive form gives us more confidence in the extrapolation of the additive form to scenarios outside of the range well constrained by the empirical data set.

EXSIM SIMULATIONS FOR LARGE-MAGNITUDE SCALING

The second issue addressed using numerical simulations is the large-magnitude scaling of the duration. The source duration term captures the effect of the rupture radiating energy over a finite time due to the risetime of the slip for each subevent and the time delay between the rupture of the subevents. For the hypocenter located in the middle of the rupture, the average source duration can be approximated by

$$D_{\text{Source}} = \frac{0.5L}{V_{\text{rup}}} + \frac{\text{Disp}_{\text{Sub}}}{V_{\text{slip}}}, \tag{11}$$

in which L is the rupture length, V_{rup} is the average rupture velocity, Disp_{Sub} is the subevent displacement, and V_{slip} is the slip velocity.

Using a magnitude–length relationship with a constant stress-drop assumption (Leonard, 2010), the magnitude–length relation is

$$L(\text{km}) = 10^{0.5(\mathbf{M}-4)}\text{AR}, \tag{12}$$

in which AR is the aspect ratio, and the displacement–magnitude relation is

$$\text{Disp}(m) = 10^{0.5(\mathbf{M}-6.86)}. \tag{13}$$

Combining equations (12) and (13) with equation (11), the source duration has the following general functional form:

$$\begin{aligned} D_{\text{Source}} &= \frac{0.5\text{AR}}{V_{\text{rup}}}10^{0.5(\mathbf{M}-4)} + \frac{10^{0.5(\mathbf{M}-6.86)}}{V_{\text{slip}}} \\ &= c_1 10^{c_2\mathbf{M}} + c_{1a}10^{c_{2a}\mathbf{M}}. \end{aligned} \tag{14}$$

For moderate-magnitude earthquakes, the magnitude slopes c_2 and c_{2a} will both be 0.5 for the constant stress-drop assumption. For large-magnitude crustal earthquakes, the rupture will reach the maximum seismogenic width ($W_{\max}$), and the AR becomes magnitude dependent ($\text{AR} = 10^{0.5(M-4)}/W_{\max}^2$).

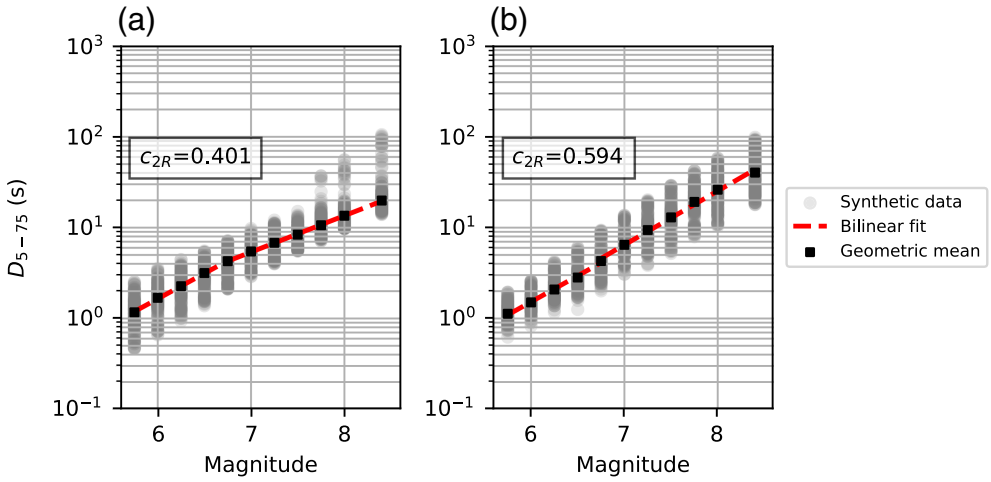

Figure 3. Magnitude scaling of D_{5-75} from the EXSIM simulations for two rupture distances. (a) $R_{Rup} = 10$ and (b) $R_{Rup} = 200$ km. The magnitude slope for **M** > 6.75, c_{2R}, is smaller for short-rupture distances due to the attenuation of the ground motions from subevents that are at large distances from the site (located at the far end of the rupture). The color version of this figure is available only in the electronic edition.

Substituting the magnitude-dependent AR into equation (12) leads to $c_2 = 1.0$. For large-magnitude events, the finite-rupture time will be much larger than the rise time of a subevent, so the c_2 term will control the magnitude scaling of the source duration.

For sites located close to long ruptures, the waves arriving at the site from the far end of the rupture will have a much smaller amplitude than the waves arriving from the nearby part of the rupture due to the attenuation with distance. The small-amplitude waves from the distant parts of the rupture will not contribute significantly to the Arias intensity. As a result, the part of the source duration that contributes to the ground-motion duration will be less than the full rupture duration (time from the start to the end of the rupture). For example, consider an **M** 8 earthquake rupturing from the San Francisco Peninsula to Eureka on the northern San Andreas fault. For a site located close to the fault rupture but near an end of the rupture, such as San Francisco, the seismic energy released at the far end of the rupture (near Eureka) will attenuate significantly as the waves propagate from Eureka to San Francisco and will not contribute significantly to the Arias intensity. Although the source radiates energy over the full rupture time, the "effective" source duration that contributes to the ground-motion duration based on the normalized I_A will be less than the full rupture time. This is the magnitude-saturation feature of the ground-motion duration for short source-to-site distances. For sites located at large distances from the rupture, the distance attenuation will be similar for the waves arriving from different locations along the rupture, so the full source duration will contribute to the ground-motion duration. As a result, we expect the source duration term to be distance dependent for large-magnitude earthquakes.

We generated synthetic ground motions for a range of magnitudes and distances using the EXSIM program (Motazedian and Atkinson, 2005) to gain insight into this behavior. For the inputs to EXSIM, we used the default source and path duration parameter values for the western United States given in Boore (2009): for the source, we adopted a stress drop of 140 bars, a shear-wave velocity at the source β of 3.7 km/s, and a rupture velocity of 0.8β. The rupture dimension is based on the scaling developed by Wells and Coppersmith (1994) for strike-slip earthquakes with a crustal thickness of 16 km. For the distance dependence of duration, we adopted the following slopes: 0 between 0 and 10 km, 0.16 between 10 and 70 km, −0.03 between 70 and 130 km, and 0.04 for distances larger than 130 km. Depending on the magnitude, the ruptures were discretized in segments ranging from 0.5 km (for the smallest magnitude) to 4 km (for the largest magnitude). We performed simulations for a suite of scenarios with magnitudes between 5.75 and 8.4, dips between 45° and 90°, and 10 hypocenters randomly distributed along the rupture. The ground motions for rupture distances (R_{Rup}) between 1 and 200 km for each scenario were computed. We did not observe a significant effect of the dip angle on the ground-motion duration.

We conducted a regression to estimate the average distance dependence of the duration from the EXSIM simulations and removed this distance scaling to isolate the source scaling. As a result, the source scaling results are not sensitive to the assumed path duration used in the EXSIM simulations, but it will depend on the geometrical spreading used in EXSIM. The resulting relationship between the D_{5-75} and magnitude is shown in Figure 3 for two R_{Rup} values: 10 and 200 km.

The EXSIM results show that the magnitude scaling has a break in the slope near magnitude 6.75. The average magnitude slope for **M** < 6.75 is 0.515, which is close to the theoretical scaling of 0.5 for a constant AR. For the 200 km case, the magnitude slope for **M** > 6.75 is 0.59, which is greater than 0.5 as expected for large-magnitude events that reach the width limit, but it is much less than 1.0 expected based on the scaling of the full rupture duration for the simple model shown in equation (14). For large-magnitude events and a rupture distance of 10 km, the magnitude slope is reduced to 0.4 due to the attenuation of the ground motion from the parts of the rupture located at large distance down strike from the site.

We modeled the magnitude slope of the source duration by a constant for moderate-magnitude earthquakes and by a distance-dependent term for large magnitudes:

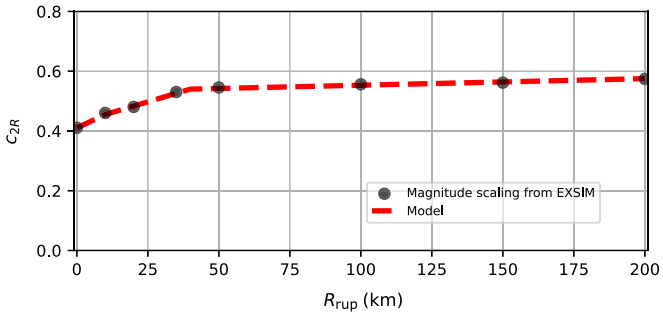

Figure 4. Distance dependence of the magnitude scaling coefficient for large-magnitude events, c_{2R}, from the results of the EXSIM simulations for D_{5-75}. The dashed line is the model for the scaling of c_{2R} to capture saturation effects for large magnitudes and short distances. The color version of this figure is available only in the electronic edition.

$$c_2(\mathbf{M},R_{\text{Rup}}) = \begin{cases} c_{2-\text{base}} & \mathbf{M} \le 6.75 \\ c_{2R}(R_{\text{Rup}}) & \mathbf{M} > 6.75 \end{cases}, \quad (15)$$

in which $c_{2-\text{base}}$ is the mean slope from magnitudes below 6.75, and $c_{2R}(R_{\text{Rup}})$ is the distance-dependent magnitude slope for $\mathbf{M} > 6.75$.

The magnitude slope from the simulated data is shown in Figure 4 for different distance bins. We adopted a trilinear model to capture the distance dependence of the large-magnitude slope due to saturation:

$$c_{2R}(R_{\text{rup}}) = \begin{cases} c_{21} + (c_{22} - c_{21})\frac{R_{\text{Rup}}}{10} & R_{\text{Rup}} \le 10 \\ c_{22} + \frac{(c_{23}-c_{22})(R_{\text{Rup}}-10)}{(40-10)} & 10 < R_{\text{Rup}} \le 40 \\ c_{23} + \frac{(c_{24}-c_{23})(R_{\text{Rup}}-40)}{(200-40)} & 40 < R_{\text{Rup}} \le 200 \end{cases}, \quad (16)$$

in which R_{Rup} is in kilometers. Because large-magnitude events at short distances are limited in our data set, we constrained the c_{21}, c_{22}, c_{23}, and c_{24} terms to the values obtained from the stochastic finite-fault simulations. The D_{5-95} values from EXSIM show a similar distance dependence of the large-magnitude slope.

DATA SET

We use a subset of the Next Generation Attenuation-West2 Project data set developed for active crustal regions (Ancheta *et al.*, 2014) for the duration data set. Starting with the subset of 15,744 records used for developing the Abrahamson *et al.* (2014) GMM, we applied three additional selection criteria. First, the data set is limited to rupture distances less than 200 km and magnitudes greater than 4.0. Second, the minimum of three recordings per earthquake and three recordings per site is required to better constrain the random effects for the source and site terms. We applied a third selection criterion for constraining the random effects for the path terms: the difference between the shortest and the largest R_{Rup} must be larger than 50 km. If the data only span a short distance range, then the event-specific distance slope cannot be reliably determined, and unrealistically large event-specific path terms can be resulted. After applying these selection criteria, the data set contains 6936 records from 109 earthquakes and 1059 sites. The magnitude–distance distribution and the V_{S30} distribution of the selected data set are shown in Figure 5.

DURATION MODEL FOR D_{5-75}

Based on the results of the 3D simulations, the functional form for D_{5-75} uses an additive form of the duration model with random effects for the source, path, and site effects.

Functional forms for the median duration

The median source term is modeled using the form in equation (14) but with a distance-dependent c_{2R} term constrained by the EXSIM simulations:

$$D_{\text{source}}(\mathbf{M},R_{\text{Rup}}) = \begin{cases} c_1 10^{c_{2-\text{base}}(\mathbf{M}-6.75)} & \mathbf{M} \le 6.75 \\ c_1 10^{c_{2R}(R_{\text{Rup}})(\mathbf{M}-6.75)} & \mathbf{M} > 6.75 \end{cases}. \quad (17)$$

In this form, the c_1 coefficient corresponds to the median duration in seconds for an **M** 6.75 earthquake recorded at short distances on a hard-rock site condition.

The path term captures the duration increase with distance due to wave scattering in the crust. Boore and Thompson (2014), Afshari and Stewart (2016), and Bahrampouri *et al.*

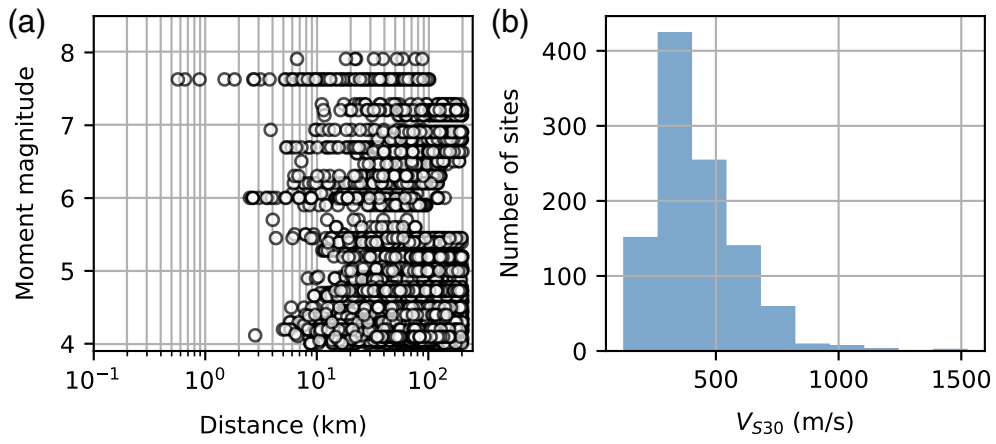

Figure 5. Distribution of the model predictors (**M**, R_{rup}, and V_{S30}) used for performing the regression. (a) The magnitude–distance distribution. (b) The V_{S30} distribution in our data set. The color version of this figure is available only in the electronic edition.

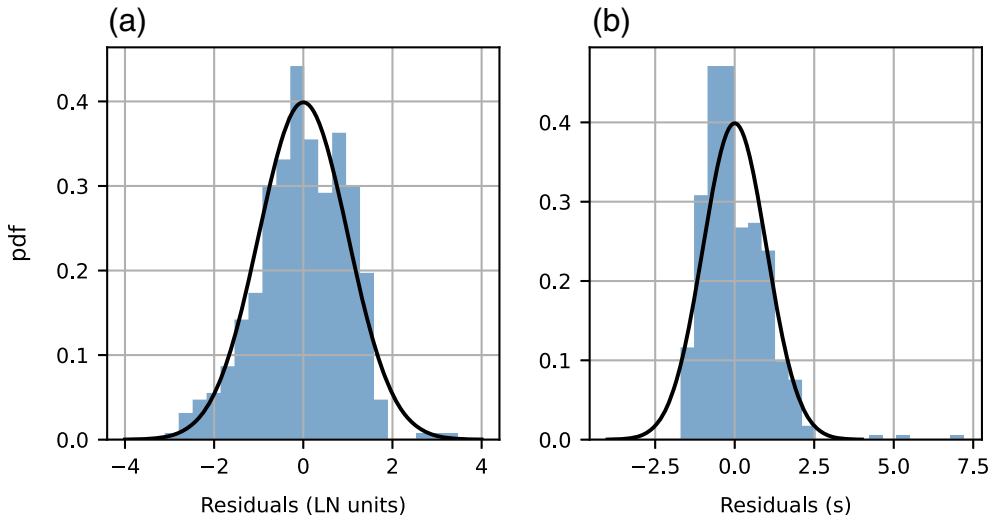

Figure 6. Distributions of the D_{5-75} duration for a subset with 30 km $< R_{rup} <$ 100 km, $5.5 < M < 6.6$, and 270 m/s $< V_{S30} <$ 350 m/s. (a) Log duration transformation and (b) linear duration. The color version of this figure is available only in the electronic edition.

We evaluated the shape of the distribution of the duration data using the D_{5-75} residuals for a limited range of magnitudes, distances, and V_{S30} values. The distributions using linear and log scales are shown in Figure 6. The distribution of linear D_{5-75} is skewed to larger values (Fig. 6b), but a log transformation leads to a distribution that is skewed to smaller values (Fig. 6a). A power transformation with an exponent between 0 and 1 leads to a skewness between normal and lognormal. Therefore, we model the duration residuals by a power-normal distribution.

In GMMs, random effects are usually included for the source and site terms to capture the correlation in the total residuals due to multiple recordings from a given source or at a given site. To constrain the duration to be positive for all values of the random effects for an additive model, the random effects are included as scale factors on the source and site terms. For the path effect, the random effect is included as a scale factor on the distance slope. The statistical form of the duration model is given by

$$(D_{5-75,es}(\mathbf{M},R_{\rm Rup},V_{S30}))^{n_1} = [D_{\rm Source}(\mathbf{M},R_{\rm Rup})e^{\delta B_e} + D_{\rm Path}(R_{\rm Rup}) + c_3 e^{\delta P_e} R_{\rm Rup} + D_{\rm Site}(V_{S30})e^{\delta S2S_s}]^{n_1} + \delta WS_{es}, \tag{20}$$

in which δB_e, δP_e, and $\delta S2S_e$ have mean zero and standard deviations of τ_S, τ_P, and ϕ_{S2S}, respectively (all in LN units); δWS_{es} is the within-event within-site residual for earthquake e recorded at site s with standard deviation ϕ_{SS}, and n_1 is the exponent that transforms δWS_{es} to a normal distribution. The units of δWS and ϕ_{SS} are s^{n1}. The c_3 term is part of the overall linear R term and scales the amplitude of the event-specific distance scaling.

For the regression, it is more stable to move the random effects out of the exponents. We use the notation Δ for the random effect that is a lognormally distributed random variable to distinguish it from the commonly used notation δ for random effects that are normally distributed. The functional form used for the regression is given by

$$(D_{5-75,es}(\mathbf{M},R_{\rm Rup},V_{S30}))^{n_1} = [\Delta B_e D_{\rm Source}(\mathbf{M},R_{\rm Rup}) + D_{\rm Path}(R_{\rm Rup}) + c_3 \Delta P_e R_{\rm Rup} + \Delta S2S_s D_{\rm Site}(V_{S30}))^{n_1} + \delta WS_{es}. \tag{21}$$

The ΔB_e, ΔP_e, and $\Delta S2S_s$ are lognormally distributed source, path, and site terms, respectively.

(2021) recognized a break in the distance scaling, and modeled the path term by bilinear or trilinear functional forms. We use the same approach, selecting a trilinear function to model the median path term:

$$D_{\rm path}(R_{\rm Rup}) = \begin{cases} c_{31}R_{\rm Rup} & R_{\rm Rup} \le R_1 \\ c_{31}R_1 + (R_{\rm Rup} - R_1)c_{32} & R_1 < R_{\rm Rup} \le R_2 \\ c_{31}R_1 + c_{32}(R_2 - R_1) + (R_{\rm Rup} - R_2)c_{33} & R_2 < R_{\rm Rup} \end{cases}. \tag{18}$$

The c_3 term captures the median crustal scaling, and the c_{3i} coefficients capture the breaks in the distance slope.

The median site term is modeled by a linear function of $\ln(V_{S30})$ with the constraint that the median site term be zero for hard-rock site conditions ($V_{S30} > V_3$). The functional form for the median site term is given by

$$D_{\rm site}(V_{S30}) = \begin{cases} c_4 \ln\left(\frac{V_{S30}}{V_3}\right) & V_{S30} \le V_3 \\ 0 & V_3 < V_{S30} \end{cases}. \tag{19}$$

Statistical form of the duration model

For the amplitudes of ground motions, the basic physical process for the source, path, and site effects can be explained by multiplicative models, and the residuals of the amplitudes are approximately log-normally distributed. In contrast, the physics behind duration scaling does not correspond to a multiplicative process of the source, path, and site effects. Therefore, the common assumption of log-normally distributed data used for amplitudes of ground motion may not apply to duration data.

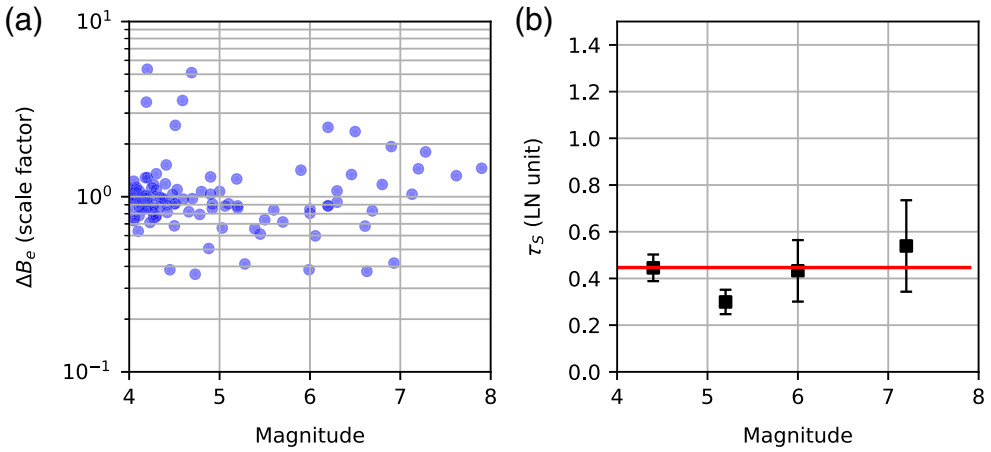

Figure 7. (a) Event terms ΔB_e as a function of **M** for D_{5-75}. (b) Standard deviation τ_S of the δB_e for D_{5-75}, binned by **M** (black squares). The error bars represent the 5th–95th confidence interval. The line is the constant τ_S for the model. The color version of this figure is available only in the electronic edition.

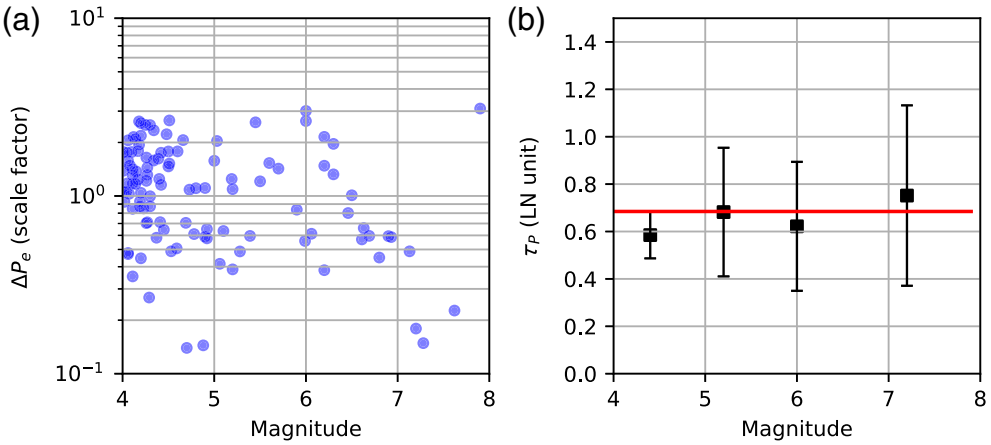

Figure 8. (a) Path terms ΔP_e as a function of **M** for D_{5-75}. (b) Standard deviation τ_P of the δp_e (ϕ_p) for D_{5-75} binned by **M** (black squares) for D_{5-75}. The error bars represent the 5th–95th confidence interval. The line is the constant τ_P for the model. The color version of this figure is available only in the electronic edition.

Event and path terms

The event terms ΔB_e are shown in Figure 7 as a function of magnitude. They do not show a trend with magnitude, indicating that the magnitude scaling from the EXSIM simulations is consistent with the magnitude scaling in the empirical data. The standard deviation of the δB is shown in Figure 7b for different magnitude bins. The variability of the δB terms does not show a clear dependence on magnitude. The variability of the δP terms shown in Figure 8 also does not show a clear dependence on magnitude. Therefore, τ_S and τ_P are modeled as magnitude-independent constants.

Site terms

The site terms and their standard deviation are shown in Figure 9 as a function of V_{S30}. There is no clear trend in the site terms with V_{S30}, indicating that the adopted functional form for the median adequately captures the V_{S30} scaling. For V_{S30} values above 300 (m/s), the ϕ_{S2S} is approximately constant; but there is a significant increase in ϕ_{S2S} for the smallest range of V_{S30}. Sites with small V_{S30} values are typically associated with deeper soil sediments and more complex basin structures. The duration for these sites will depend on the direction of the waves entering the basin, which will lead to larger variability in the duration values for sites in basins. Therefore, we consider the observation of an increase in ϕ_{S2S} for soft sites to be physically reasonable and included it in our model.

We modeled ϕ_{S2S} with a piece-wise linear model:

$$\phi_{S2S} = \begin{cases} \phi_1 & V_{S30} \le V_1 \\ \phi_0 + (\phi_1 - \phi_0)\left(\frac{\ln(V_2)-\ln(V_{S30})}{\ln(V_2)-\ln(V_1)}\right) & V_1 < V_{S30} \le V_2 \\ \phi_0 & V_2 < V_{S30} \end{cases}. \quad (22)$$

REGRESSION RESULTS

We used the functional form in equation (21) to model the D_{5-75} data set. The problem becomes a complex nonlinear mixed-effects regression in which the random effects are lognormally distributed factors for the additive terms, and the sum is raised to the power n_1. We conducted a nonlinear regression based on a Bayesian approach using the Python module pymc3 (Salvatier *et al.*, 2016). We adopted uniform distributions for the model coefficients to add noninformative and unbiased prior distributions. To determine the exponent n_1 for the power transformation, n_1 values between 0 and 0.85 were tested. A n_1 value of 0.7 was selected, because it lead to a skewness of δWS that is close to zero (Fig. S5).

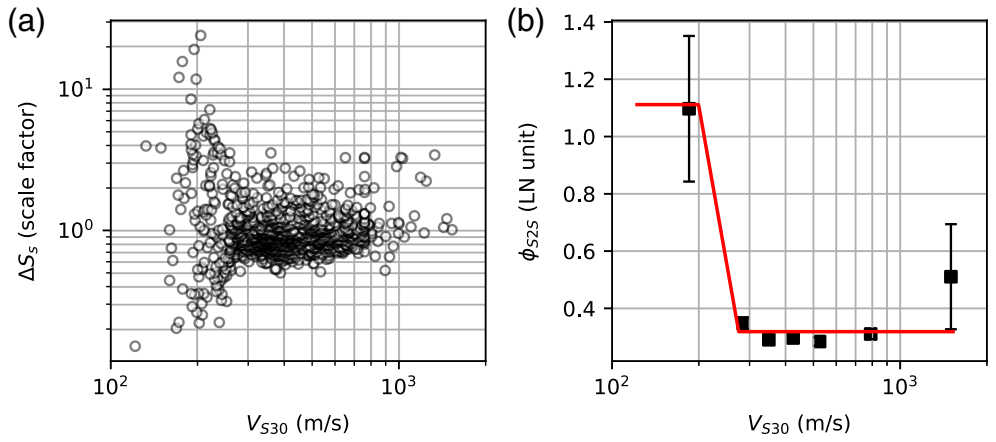

Figure 9. (a) Site terms ΔS as a function of V_{S30} for D_{5-75}. (b) Standard deviation ϕ_{S2S} of the $\delta S2S$ for D_{5-75} binned by V_{S30} (black squares). The error bars represent the 5th–95th confidence interval. The line is the model for ϕ_{S2S} accounting for the increased variability for softer sites. The color version of this figure is available only in the electronic edition.

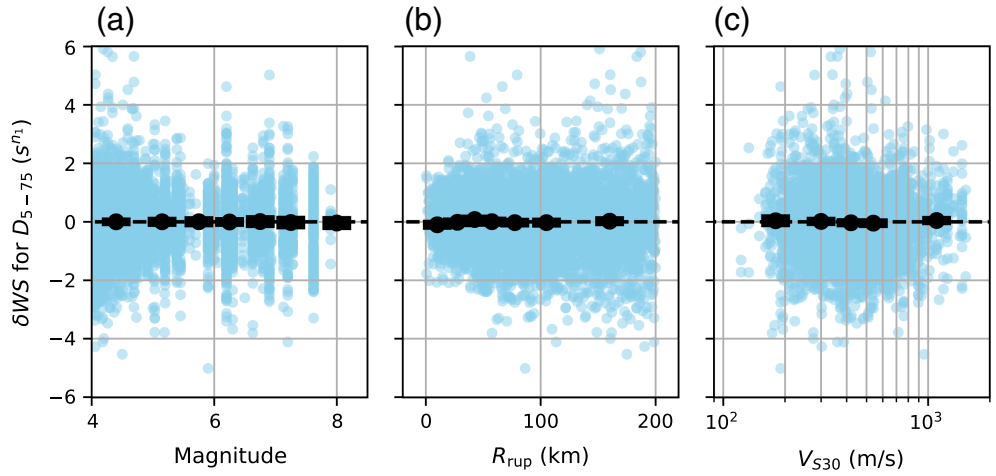

Figure 10. Within-site residuals for D_{5-75} as a function of magnitude R_{rup} and V_{S30}. (a) Magnitude dependence. (b) Distance dependence. (c) V_{S30} dependence. The black points and error bars are the mean and the 5%–95% confidence interval of the mean for each bin, respectively. The color version of this figure is available only in the electronic edition.

The model for the V_{S30} dependence of ϕ_{S2S} is shown in Figure 9b. The site random effects are assumed to be lognormally distributed, but from the Bayesian regression, the site random effects are slightly different from lognormal, and the mean of the ϵ_s is nonzero. To avoid a bias in the model, we include the mean ϵ_s, denoted s_1, in the median model as a factor, $\exp(s_1\phi_{S2S})$, on the site term.

Within-site residuals

The magnitude, distance, and V_{S30} dependence of the within-site residuals δWS for the D_{5-75} models are shown in Figure 10. There are no clear trends in the δWS with magnitude, distance, or V_{S30}. The δWS are shown as a function of V_{S30} for different magnitude bins in Figure 11. The lack of trends in residuals for different magnitudes indicates that the site terms are independent of magnitude and supports the use of the additive model for the site terms. We also evaluated the δWS for nonlinear site effects. The residuals for soil sites with $V_{S30} < 270$ m/s do not show a dependence on the amplitude of the input peak ground acceleration (PGA) (Fig. S6), indicating that the empirical data do not show nonlinear site effects on the D_{5-75}. We evaluated the saturation for large-magnitude events at short distances, using the residuals for $\mathbf{M} \geq 7$ for $R_{\mathrm{Rup}} < 30$ km. The mean residual for this subset is 0.55, but this nonzero residual is due to the uneven sampling of the rupture direction in the data set and not to a bias in the saturation model. For large magnitudes and short distances, the duration is sensitive to direction of the rupture. The parameter s/L is the fraction of the rupture toward the site, in which s is the length of rupture between the site and the epicenter, and L is the total length of the rupture. The ground-motion duration due to the finite rupture of the source will be the largest for $s/L = 0$ (rupture away from the site) and the smallest for $s/L = 1$ (unilateral rupture toward the site). For a randomly located site within 30 km of the rupture and a uniform distribution of hypocenters along strike, the mean value of s/L is 0.4. There is a strong s/L dependence of the large-magnitude short-distance residuals (Fig. S9), but the mean residual for $s/L = 0.4$ is near zero, indicating that the saturation model is centered (unbiased) for a future earthquake and a uniform sample of the near-fault site locations.

The distribution of the δWS residuals was evaluated using Q-Q plots (Fig. S7). For epsilon values between −2 and 2, the epsilon are consistent with the a normal distribution.

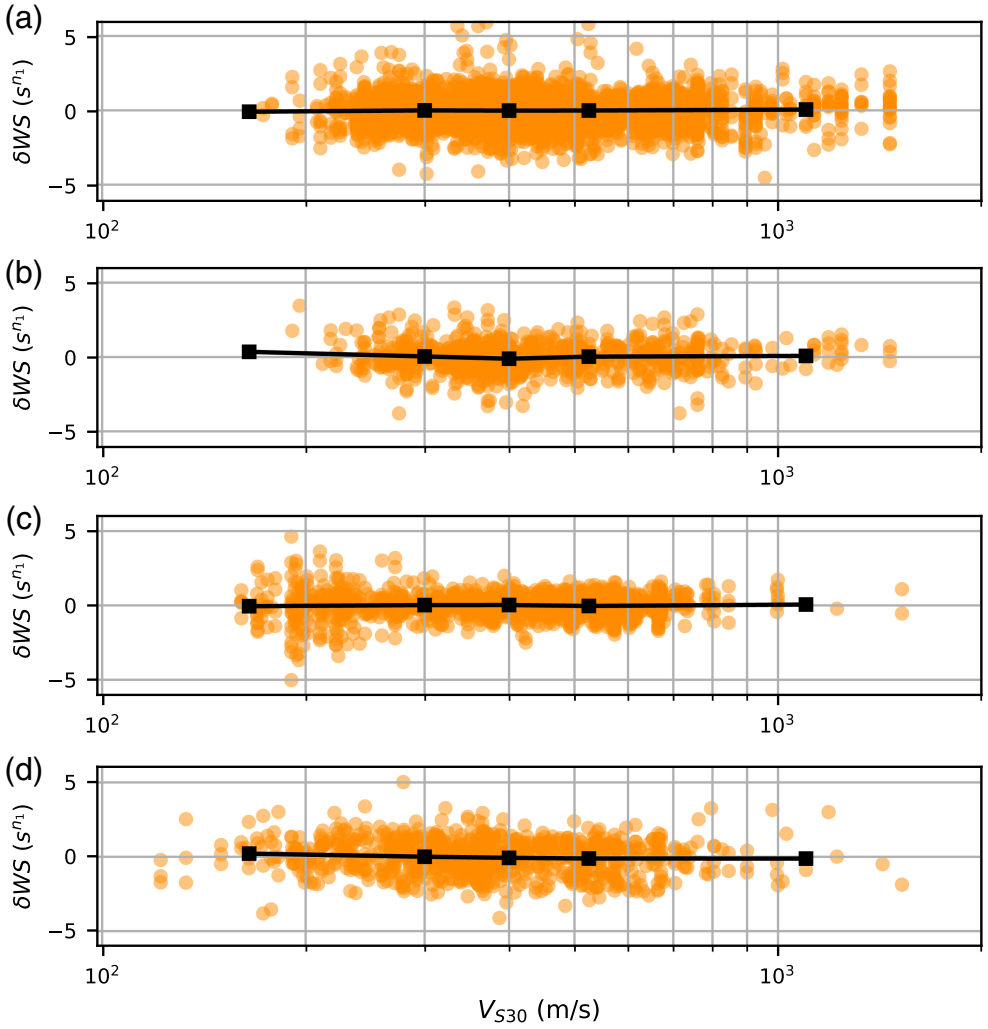

Figure 11. Within-site residuals for D_{5-75} as function of V_{S30} for different magnitude ranges. (a) **M** 4.0–4.8. (b) **M** 4.8–5.5. (c) **M** 5.5–6.5. (d) **M** 6.5–8.0. The black points are the mean for each bin. The color version of this figure is available only in the electronic edition.

Functional form for D_{5-75}

The final functional form for D_{5-75} is given by

$$(D_{5-75,es})^{n_1} = [\Delta B_e D_{\text{source}}(\mathbf{M}, R_{\text{rup}}) + D_{\text{Path}}(R_{\text{rup}}) + c_3 \Delta P_{es} R_{\text{rup}} + c_4 \Delta S2S_s \ln\left(\frac{V_{S30-s}}{V_3}\right) e^{s_1 \phi_{S2S}(V_{S30})}]^{n_1} + \delta WS_{es}. \quad (23)$$

The resulting coefficients for the D_{5-75} model are listed in Table 1. For the median model, the ΔB, ΔP, and $\Delta S2S$ are set to unity.

MODEL SIMPLIFICATION FOR PREDICTIONS

The duration model includes four random variables: the site term ($\Delta S2S_s$), the event term (ΔB_e), the path term (Δ_p), and the within-site residual (δWS_{es}). The $\Delta S2S_s$, and parts of Δ_p and ΔB_e can be included as systematic effects in a non-ergodic form of the model; however, these three random variables are treated as part of the aleatory variability for an ergodic model. Because of the form of the duration model, the standard deviation for

TABLE 1
Model Coefficients for the D_{5-75} Duration Model

Source Terms		Path Terms		Site Terms		St. Dev. Terms	
Equations (15)–(17)		**Equation (18)**		**Equation (19)**		**Full Model**	
Coefficient	**Value**	**Coefficient**	**Value**	**Coefficient**	**Value**	**Coefficient**	**Value**
c_1	3.655	c_3	0.041	c_4	−0.619	τ_s(ln)	0.447
c_{2-base}	0.515	c_{31}	0.063	s_1	0.278	τ_p(ln)	0.685
c_{21}	0.41	c_{32}	0.034	V_3 (m/s)	2000	φ_{S2S}(ln)	Equation (22)
c_{22}	0.455	c_{33}	0.083	–	–	φ_0(ln)	0.565
c_{23}	0.54	R_1	44	–	–	φ_1(ln)	1.111
c_{24}	0.575	R_2	130	–	–	$\varphi_{SS}(s^{0.3})$	1.45
–	–	–	–	–	–	V_1 (m/s)	200
–	–	–	–	–	–	V_2 (m/s)	275
–	–	–	–	–	–	n_1	0.7

these four terms cannot be analytically combined into a total standard deviation as is done for GMMs for PSA. To provide a simplified model for the total standard deviation, we numerically sampled the four random variables and developed an approximate distribution for the total residual and the within-event residual (without the ΔB and ΔP). The sampling covered magnitudes between 4.8 and 8.1, distances between 0 and 200 km, and V_{S30} between 160 and 2000.

The correlation of the site, path, and source random effects is weak (Fig. S8). For simplicity, we sampled the random effects independently. The $\delta S2S_s$, δP_{es}, δB_e, and δWS_{es} were sampled from normal distributions with mean 0 with standard deviation ϕ_{S2S}, τ_P, τ_S, and ϕ_{SS}, respectively.

The total residuals δ_{es} from the simulated data are given by

$$\delta_{es}(\vec{x}) = ((D(\vec{x},\Delta S2S_s,\Delta B_e,\Delta P_e)^{n_1} + \delta WS_{es})^{\frac{1}{n_1}})^{n_2} - (D_{\text{med}}(\vec{x}))^{n_2}, \quad (24)$$

in which $D_{\text{med}}(\vec{x})$ is the median value of our model, given a set of input parameters $\vec{x} = (\mathbf{M},R_{\text{rup}},V_{S30})$. We found the exponent n_2 for a power transformation that led to an approximately normal distribution for δ_{es} (see Table 1). The best exponent for the power normal transformation is for $n_2 = 0.3$, whereas the best power-normal distribution of the δWS was $n_1 = 0.7$. The exponent for the power-normal transformation for the total residual is smaller than for the within-site residual due to the inclusion of the $\delta S2S_s$, δP_e, and δB_e terms, in addition to the δWS in the total residuals.

We evaluated the magnitude, distance, and V_{S30} dependence of the standard deviation of δ and found trends with magnitude, distance, and V_{S30} (Fig. S10). To model these trends, the functional form for the total standard deviation is given by

$$\sigma_{5-75} = a_0 + a_1\frac{R}{100} + a_2\left(\frac{R}{100}\right)^2 + b_1\mathbf{M} + b_2\mathbf{M}^2 + \text{Min}\left[d_1\left(\frac{V_4}{V_{S30}}\right)^{d_2},d_3\right]. \quad (25)$$

The σ_{5-75} is in units of $s^{0.3}$. The coefficients are listed in Table 2.

The power-normal distribution can lead to negative values of lower tail of $D_{5-75}^{0.3}$, which is undefined if converted back to arithmetic units. For the simplified model, we truncate the lower tail of the normal distribution of $D_{5-75}^{0.3}$ at zero. The D_{5-75} is modeled through a lower truncated normal distribution (LTN) by

$$D_{5-75} \sim (\text{LTN}(\mu^{n_2},\sigma_{5-75}^2))^{\frac{1}{n_2}}, \quad (26)$$

in which

$$\mu_{5-75}(s) = c_1 10^{c_2(R_{\text{Rup}})(\mathbf{M}-6.75)} + D_{\text{Path}}(R_{\text{rup}}) + c_3R_{\text{Rup}} + c_4\ln\left(\frac{V_{S30}}{V_3}\right)e^{s_1\phi_{S2S}(V_{S30})}. \quad (27)$$

TABLE 2
Coefficients for the Simplified Standard Deviation Model for D_{5-75} (Equation 25)

Coefficient	$\sigma_{5-75}(s^{0.3})$	$\varphi_{5-75}(s^{0.3})$
a_0	0.537	0.099
a_1	−0.093	−0.152
a_2	0.0278	0.0334
b_1	−0.0372	0.116
b_2	0.00179	−0.0115
d_1	0.0206	0.0301
d_2	2.401	2.525
d_3	0.0419	0.0626
V_4	200	200
n_2	0.3	0.3

Correlation with PGA residuals

If the same seismic energy is compacted into a shorter duration, then the amplitude will be larger. Therefore, we expect the duration residuals to be negatively correlated with the PGA residuals. Using the normalized total residuals of ln(PGA) and $D_{5-75}^{0.3}$, we computed the correlation coefficient $\rho(\epsilon_{\text{lnPGA}},\epsilon_{D575})$. There is a negative correlation with $\rho(\epsilon_{\text{lnPGA}},\epsilon_{D575}) = -0.57$ (Fig. S11). We found no magnitude dependence of the correlation coefficient. In seismic hazard applications, the median and standard deviation of the duration conditioned on the ϵ_{PGA} are given by

$$D_{5-75\text{med}}(\epsilon_{\text{lnPGA}}) = \mu_{5-75}^{0.3} + \rho(\epsilon_{\text{lnPGA}},\epsilon_{D575})\epsilon_{\text{lnPGA}}\sigma_{5-75}, \quad (28)$$

$$\sigma_{5-75}(\epsilon_{\text{lnPGA}}) = \sigma_{5-75}\sqrt{1-\rho^2(\epsilon_{\text{lnPGA}},\epsilon_{D575})}. \quad (29)$$

INTERDURATION MODEL

In addition to a model for the standard duration D_{5-75} metric, we develop a model for the evolution of the normalized I_A over time by combining the observed D_{5-75} with the $\frac{D_{5-X}}{D_{5-75}}$ ratio:

$$D_{5-X,es} = D_{5-75,es}\left(\frac{D_{5-X}}{D_{5-75}}\right)_{es}. \quad (30)$$

The $\frac{D_{5-X}}{D_{5-75}}$ ratios are shown in Figure 12 as a function of the X value. The observed $D_{5-75,es}$ term captures most of the magnitude, distance, and V_{S30} scaling for the D_{5-X}, but there is still some dependence of the ratio on R_{Rup} and V_{S30}, as shown in Figure 13. The magnitude dependence of the ratio is weak, with only a difference for the $\mathbf{M}$ <5.5 range.

The distance dependence of the ratio is significant at small and intermediate values of X, with larger ratios for larger distances. This distance dependence can be explained by the difference of the P-wave's and S-wave's arrival time for short and large distances. If the 5% I_A level is reached during the P-wave

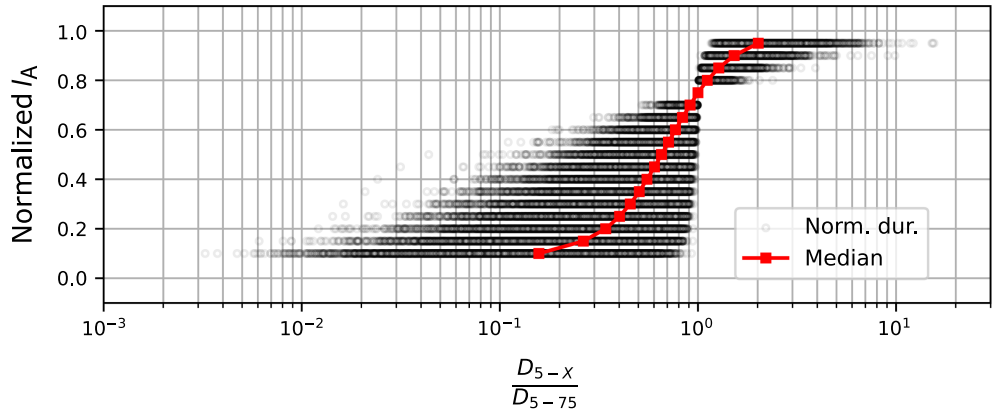

Figure 12. $\frac{D_{5-X}}{D_{5-75}}$ ratio from our data set for different normalized I_A levels. The black squares are the median for each X value. The color version of this figure is available only in the electronic edition.

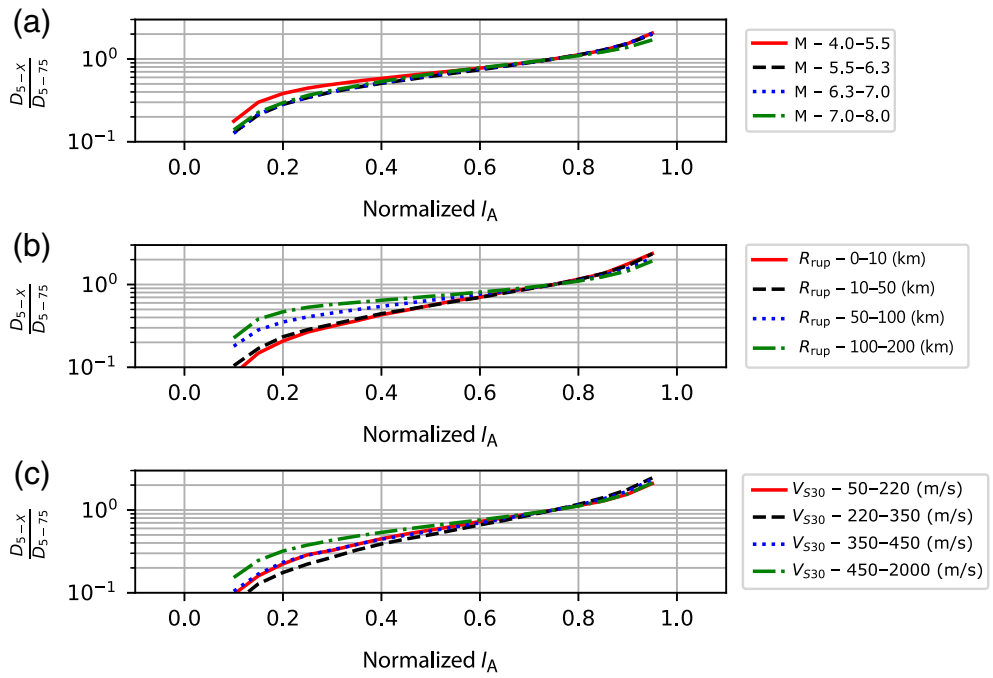

Figure 13. $\frac{D_{5-X}}{D_{5-75}}$ ratio binned by the three input parameters. (a) Data binned by magnitude. (b) Data binned by the R_{Rup}. (c) Data binned by V_{S30}. The color version of this figure is available only in the electronic edition.

phases and the 10% or larger I_A levels are reached during the S-wave's phases, then the longer S–P-wave times will lead to larger $\frac{D_{5-X}}{D_{5-75}}$ ratios for larger distances.

The V_{S30} dependence of the ratio is also the strongest at the small and intermediate values of X with larger ratios for larger V_{S30} values. A possible cause for larger ratios for rock sites is that the high-frequency P waves are attenuated due to damping for soil sites, so the I_A does not reach the 5% level until the S-wave arrival for softer sites, whereas, with less damping of the high-frequency P waves for rock sites, the I_A for rock sites may reach the 5% level during the P waves. If the S-P time contributes to the D_{5-X} for rock sites but not for soil sites, the $\frac{D_{5-X}}{D_{5-75}}$ ratio will increase for rock sites.

The $\frac{D_{5-X}}{D_{5-75}}$ ratio values are modeled by a beta distribution with probability density function given by

$$\beta_{\text{pdf}} = \frac{x^{\alpha-1}(1-x)^{\beta-1}}{\frac{\Gamma(\alpha)\cdot\Gamma(\beta)}{\Gamma(\alpha+\beta)}}, \quad (31)$$

in which Γ is the Gamma function, and x is the normalized ratio given by

$$x = \frac{\left(\frac{D_{5-X}}{D_{5-75}}\right)}{x_f - x_0}. \quad (32)$$

The parameters α, β, x_0, and x_f are given in Table 3. We found that the D_{5-X} values can be approximated by a power-normal distribution with exponent of 0.3 for all X values. To estimate the R_{Rup} and V_{S30} scaling for D_{5-X}, the regression was conducted for the $D_{5-X}^{0.3}$ values rather than for the ratio values using a conditional GMM approach in which the observed D_{5-75} is an input.

The magnitude, distance, and V_{S30} dependence of the $D_{5-X}^{0.3}$ residuals is shown in Figure 14 for X = 20, 40, and 90. We used a simple linear dependence of the $D_{5-X}^{0.3}$ with distance and $\ln(V_{S30})$:

$$D_{5-X,es}^{0.3} = D_{5-75}(\vec{X})^{0.3}(C_{\text{med}}(X) + a_0 + r_{1x}R_{\text{Rup}} + v_{1x}\ln\left(\frac{V_{S30}}{2000}\right))^{0.3} + \delta WS_{5-X,es}, \quad (33)$$

in which $C_{\text{med}}(X)$ is the median $\frac{D_{5-X}}{D_{5-75}}$ ratio from the beta distribution at energy level X. The coefficients for equation (33) are listed in Table 4.

To simplify the notation, we define C as the ratio and $f(x)$ as the transformed D_{5-X}:

$$C(\vec{x},X) = C_{\text{med}}(X) + a_0 + r_{1x}R_{\text{Rup}} + v_{1x}\ln\left(\frac{V_{S30}}{2000}\right), \quad (34)$$

$$f(\vec{x},X) = D^{0.3}_{5-X}(\vec{x}) = D^{0.3}_{5-75}(\vec{x})C^{0.3}(\vec{x},X). \quad (35)$$

The variance of $D^{0.3}_{5-X}$ can be computed by simple propagation of errors with two random variables:

$$\sigma^2_{5-X} = \sigma^2_{D5-75}\left(\frac{\partial f}{\partial D^{0.3}_{5-75}}\right)^2 + \sigma^2_C\left(\frac{\partial f}{\partial C}\right)^2 + 2\rho(D^{0.3}_{5-75},C)\sigma_{D5-75}\sigma_C\frac{\partial f}{\partial D^{0.3}_{5-75}}\frac{\partial f}{\partial C}, \quad (36)$$

in which σ_{D5-75} and σ_C are the standard deviations of $D^{0.3}_{5-75}$ and C, respectively, and $\rho(D^{0.3}_{5-75},C)$ is the correlation coefficient between $D^{0.3}_{5-75}$ and the C. With the partial derivatives of equation (35), the standard deviation is given by

$$\sigma^2_{5-X} = \sigma^2_{D5-75}C^{0.6}(\vec{x}) + 0.09\sigma^2_C D^{0.6}_{5-75}C(\vec{x})^{0.6-2} + 0.6\rho(D^{0.3}_{5-75},C)C^{0.6-1}(\vec{x})D^{0.3}_{5-75}\sigma_{D5-75}\sigma_C. \quad (37)$$

The values for σ_C and $\rho(D^{0.3}_{5-75},C)$ are listed in Tables 3 and 4, respectively.

COMPARISON WITH CURRENT MODELS

A summary of the magnitude, distance, and V_{S30} scaling in our model is shown in Figure 15. A key feature of the additive model is that the site effect on duration is a small part of the total duration for large magnitudes or large distances. At short distances, the duration is mainly affected by the magnitude, but the duration is mainly affected by the source-to-site distance at large distances.

We compare the predictions of our model with two recent duration models: Afshari and Stewart (2016; hereafter, AS16) and Bahrampouri *et al.* (2021; hereafter, BRG21). The median prediction is shown in Figure 16 as a function of magnitude at a fixed distance and site condition. At 10 km distance, the slope of the curve for the AS96 and BRG21 models for **M** 7.2–8 is much steeper than the slope for our model, showing the effect of the constraint from the EXSIM finite-source simulations. At 100 km, the median duration for large magnitudes for our model is similar to the median duration for the AS16 and BRG21. At this distance, there is no large-magnitude saturation.

The distance scaling for the duration models is compared in Figure 17. Near the center of the data (V_{S30} = 400 m/s and **M** 6.0, and R_{RUP} = 75 km), the alternative models give similar median duration values. The saturation derived from the EXSIM simulations is clearly seen in the lower plot (**M** 8.0): at distances less than 40 km, the saturation leads to a change in the slope with distance for the **M** 8 case, which is not included in the other two models.

The V_{S30} scaling from the three models is compared in Figure 18. To emphasize the V_{S30} scaling, we show the difference in the duration relative to the duration for a soft-rock site condition with V_{S30} = 760 m/s. The use of an additive functional form for the site term in our model leads to a difference

TABLE 3
Parameters for Characterizing the Beta Distribution (Equations 31 and 32) and the Power Normal Distribution for $(\frac{D_{5-X}}{D_{5-75}})^{n2}$ for *X* Values Between 10 and 95

	Beta Distribution						Power Normal ($n_2 = 0.3$)	
X	α	β	x_0	x_f	Median μ_C	St. Dev. σ_C	St. Dev. σ_{PN}	Skewness γ
0.10	1.256	4.969	0	1	0.157	0.156	0.395	0.150
0.15	1.506	3.484	0	1	0.264	0.192	0.406	0.041
0.20	1.762	3.026	0	1	0.342	0.205	0.401	–0.003
0.25	2.074	2.879	0	1	0.402	0.206	0.394	–0.066
0.30	2.436	2.836	0	1	0.455	0.202	0.379	–0.067
0.35	2.88	2.837	0	1	0.505	0.195	0.371	–0.100
0.40	3.418	2.846	0	1	0.553	0.187	0.363	–0.093
0.45	4.085	2.845	0	1	0.603	0.177	0.356	–0.117
0.50	5.035	2.88	0	1	0.654	0.163	0.346	–0.139
0.55	6.466	2.931	0	1	0.710	0.146	0.344	–0.137
0.60	8.709	2.946	0	1	0.769	0.125	0.340	–0.163
0.65	12.993	2.922	0	1	0.835	0.097	0.337	–0.161
0.70	24.082	2.705	0	1	0.912	0.060	0.339	–0.197
0.75	–	–	–	–	1	0	–	–
0.80	2.724	77.919	1	4	1.114	0.089	0.365	–0.196
0.85	2.927	69.172	1	8	1.273	0.210	0.392	–0.095
0.90	2.836	51.306	1	12	1.522	0.434	0.438	–0.005
0.95	2.721	58.393	1	28	2.014	0.907	0.525	0.107

γ is the distribution skewness for a power normal transformation with exponent 0.3.

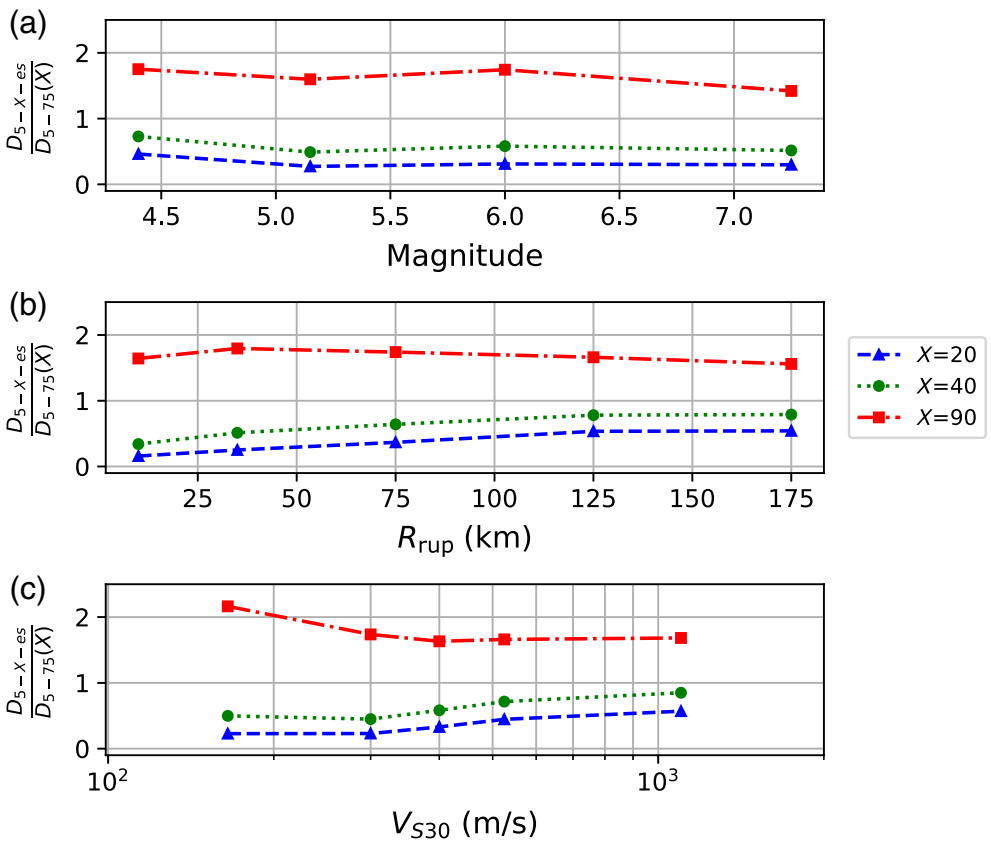

Figure 14. Residuals of $D^{0.3}_{5-20}$ relative to a constant median for the $\frac{D_{5-X}}{D_{5-75}}$ ratio for $X = 20$, 40 and 90. (a) Data binned by magnitude. (b) Data binned by distance. (c) Data binned by V_{S30}. The color version of this figure is available only in the electronic edition.

in the duration of only a few seconds between stiff and soft sites for all magnitudes and distances. For magnitude 6, the V_{S30} scaling from soft-rock to soil sites for all three models are consistent, ranging between 2 and 3 s. In contrast, at magnitude 8, the site term for our model remains at 2–3 s, whereas the BRG21 and AS16 models have a difference of 8 and 15 s between stiff and soft sites, respectively. This large difference is a consequence of the use of a multiplicative site term in the BRG21 and AS16 models.

Comparisons of our D_{5-95} duration model with existing models show similar differences as seen for the D_{5-75} duration (Figs. S12–S14).

The ratios of the 84th percentile to the median and the 16th percentile to the median for the three models are compared in Figure 19. The power-normal distribution for our model leads to a narrower

TABLE 4
Coefficients for the Median Adjustment of the D_{5-X} Model (Equation 33)

Normalized I_A	C_{med}	a_0	r_{1x}	v_{1x}	$\rho\left(D^{0.3}_{5-75}, C\right)$
0.05	0.000	0.000	0.000	0.000	0.000
0.1	0.157	−0.010798	0.0007	0.0390	-0.083
0.15	0.264	−0.016831	0.0012	0.0656	0.022
0.2	0.342	−0.012831	0.0014	0.0852	0.078
0.25	0.402	0.002943	0.0015	0.1001	0.113
0.3	0.455	0.022670	0.0015	0.1134	0.137
0.35	0.505	0.047579	0.0014	0.1259	0.154
0.4	0.553	0.076718	0.0013	0.1377	0.167
0.45	0.603	0.107148	0.0012	0.1501	0.178
0.5	0.654	0.136351	0.0010	0.1587	0.188
0.55	0.710	0.115442	0.0008	0.1365	0.198
0.6	0.769	0.092914	0.0007	0.1105	0.206
0.65	0.835	0.067803	0.0005	0.0800	0.209
0.7	0.912	0.034992	0.0002	0.0428	0.204
0.75	1.000	1.000	0.000	0.000	0.000
0.8	1.114	−0.044725	−0.0003	−0.0512	−0.301
0.85	1.273	−0.112447	−0.0006	−0.1197	−0.361
0.9	1.522	−0.209689	−0.0010	−0.2111	−0.403
0.95	2.014	−0.380920	−0.0015	−0.3589	−0.452

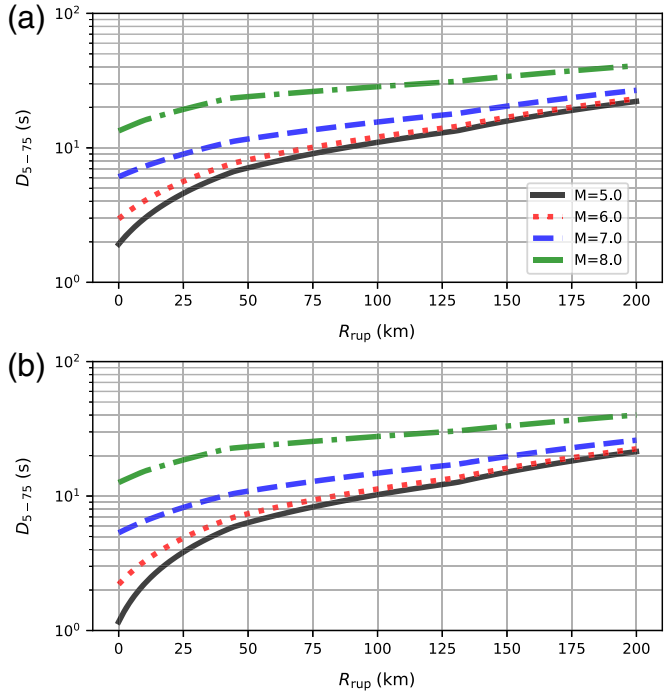

Figure 15. Example of the distance scaling of the proposed D_{5-75} model for a set of magnitudes. (a) $V_{S30} = 270$ and (b) $V_{S30} = 760$ m/s. The color version of this figure is available only in the electronic edition.

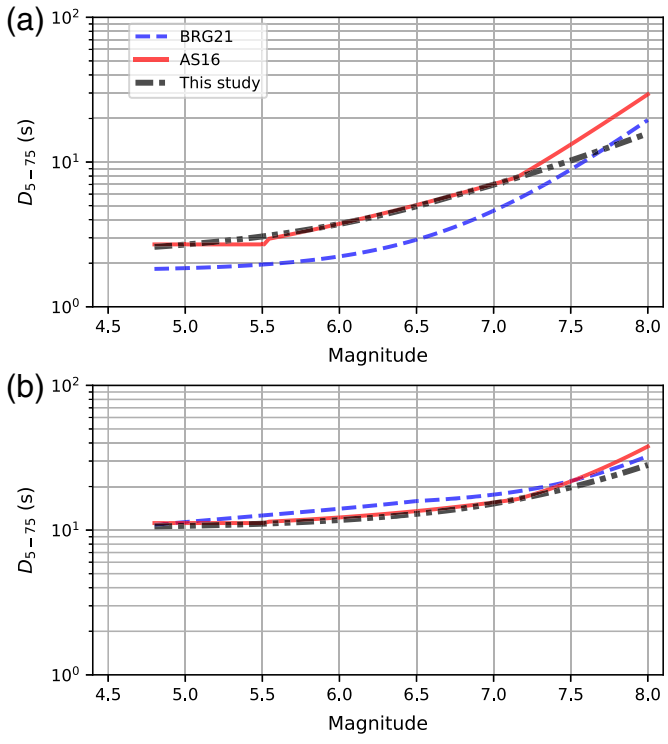

Figure 16. Comparison of the magnitude scaling of the D_{5-75} model with current models. (a) $R_{rup} = 10$ km, $V_{S30} = 400$ m/s and (b) $R_{RUP} = 100$ km, $V_{S30} = 400$ m/s. The color version of this figure is available only in the electronic edition.

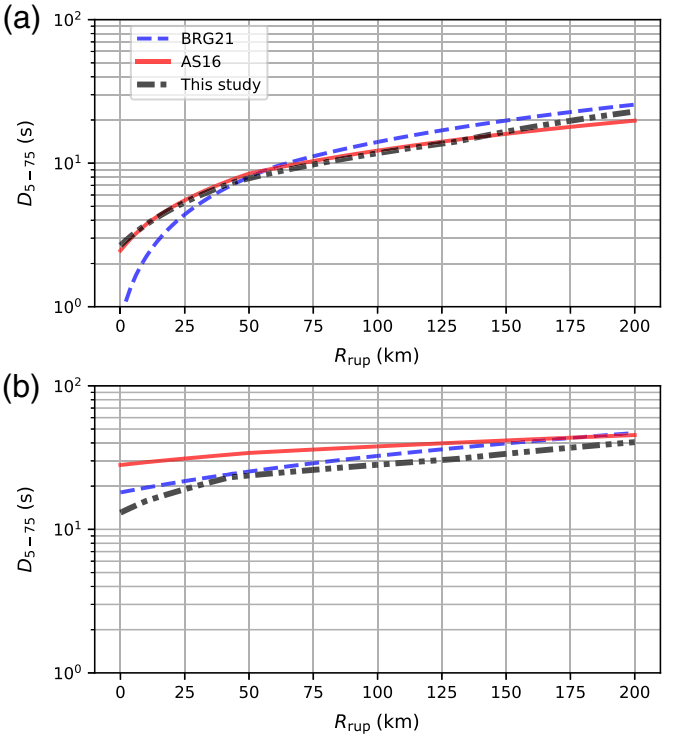

Figure 17. Comparison of the distance scaling of the D_{5-75} model with current models. (a) **M** 6, $V_{S30} = 400$ m/s and (b) **M** 8, $V_{S30} = 400$ m/s. The color version of this figure is available only in the electronic edition.

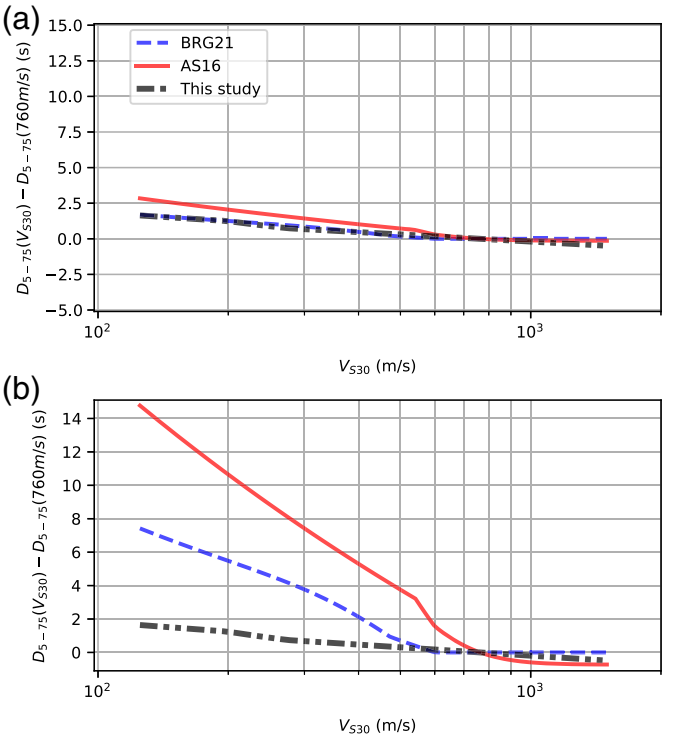

Figure 18. Comparison of the V_{S30} scaling of the D_{5-75} model with current models. (a) **M** 6, $R_{rup} = 30$ km and (b) **M** 8, $R_{RUP} = 30$ km. The color version of this figure is available only in the electronic edition.

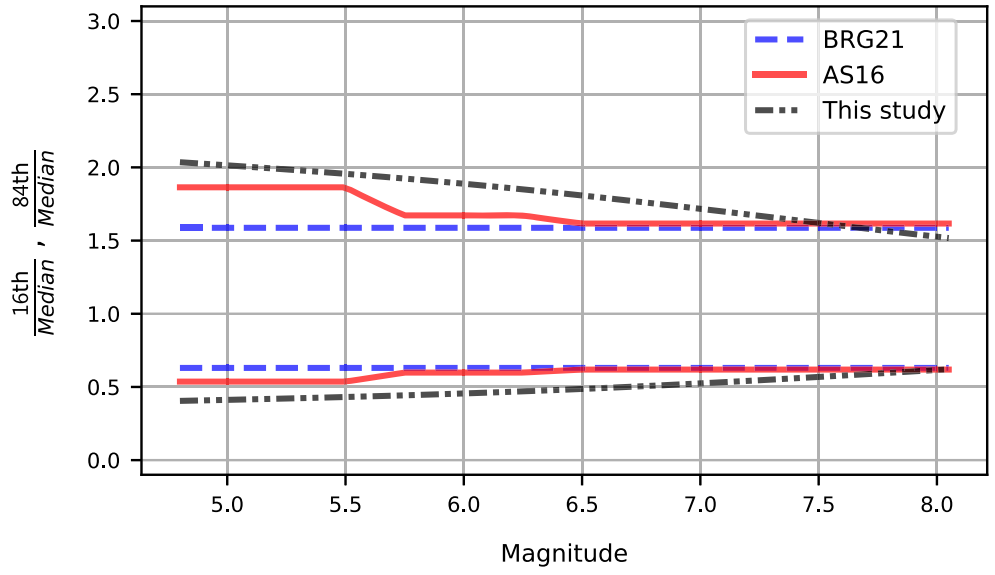

Figure 19. Comparison of the 16th median ratio and the 84th median ratio for Afshari and Stewart (2016; referred as AS16), Bahrampouri *et al.* (2021; referred as BRG21) and our model. Results are shown for $V_{S30} = 400$ m/s and $R_{rup} = 30$ km. The color version of this figure is available only in the electronic edition.

aleatory variability range at large magnitudes and large distances and a larger aleatory variability at short distances and small magnitudes as compared to the AS16 and BRG21 models, which assume a log-normal distribution of residuals.

Our model for the $\frac{D_{5-X}}{D_{5-75}}$ ratio is compared to the ratio from the Silva *et al.* (1996; hereafter, AS96) model in Figure 20 for an M 7 earthquake at a distance of 30 km. Although the AS96 model was developed from a much smaller data set, the median normalized shape and the standard deviation of the shape are similar for the new model and the AS96 model for this scenario.

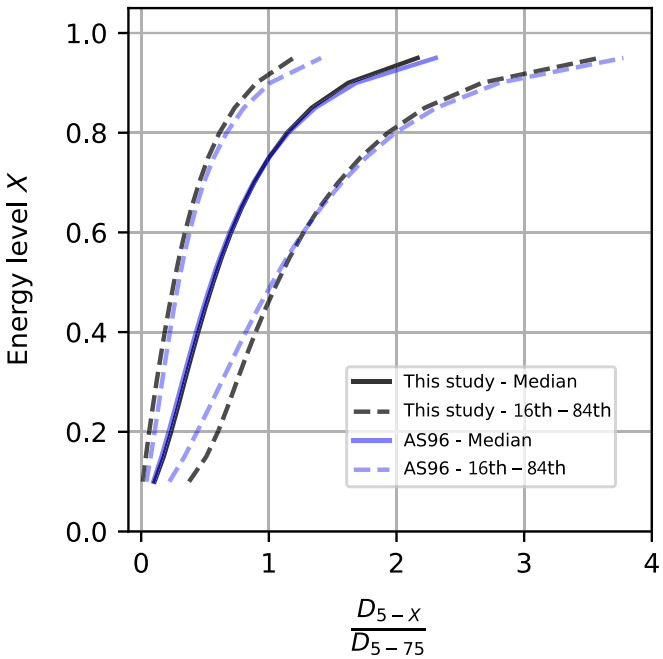

Figure 20. Comparison of the interduration model with the AS96 model for **M** 7, $V_{S30} = 400$ m/s, and $R_{RUP} = 30$ km. The color version of this figure is available only in the electronic edition.

Finally, we tested our model using the preliminary D_{5-95} duration values from the two large earthquakes in Türkiye in February 2023: the **M** 7.8 Kahramanmara and **M** 7.7 Adana earthquakes. The D_{5-95} duration data are from Cetin *et al.* (2023). The comparisons of the model and the observed D_{5-95} data are shown in Figure 21. The source random effects are 0.887 and 1.004 for the magnitude 7.7 and 7.8 events, respectively. These source terms are not far from unity, indicating that large-magnitude source scaling in our model is consistent with the observations from the two large earthquakes in the Türkiye 2023 sequence. The path random effects are 0.668 and 0.931 for the magnitude 7.7 and 7.8 events, respectively. The smaller value of 0.668 for the **M** 7.7 event indicates weaker distance scaling (less scattering) for this event as compared to the global model. For comparisons with data from a single event, the standard deviation is shown without event terms ΔB and ΔP. The event-specific path random effect captures the systematic differences in the wave scattering for this region as compared to the global model. Overall, our model is consistent with the duration data from these two large strike-slip events.

CONCLUSIONS

The numerical simulations for a simple 3D crustal structure show that the additive form for the source, path, and site effects on duration has a better physical basis than a multiplicative form for the site. An additive form for the site term leads to site effects that are independent of magnitude and distance.

The finite-fault simulations show that there is a saturation of the large-magnitude scaling of duration at short distances. This change in the magnitude scaling leads to a reduction in the median duration of about a factor of 2, as the model is extrapolated from **M** 7 to 8 earthquakes at short distances as compared to current models. With the constraints from the analytical modeling, we have more confidence in extrapolating the duration model outside the range well constrained by the data to large-magnitude short-distance scenarios that often control the seismic hazard in active regions.

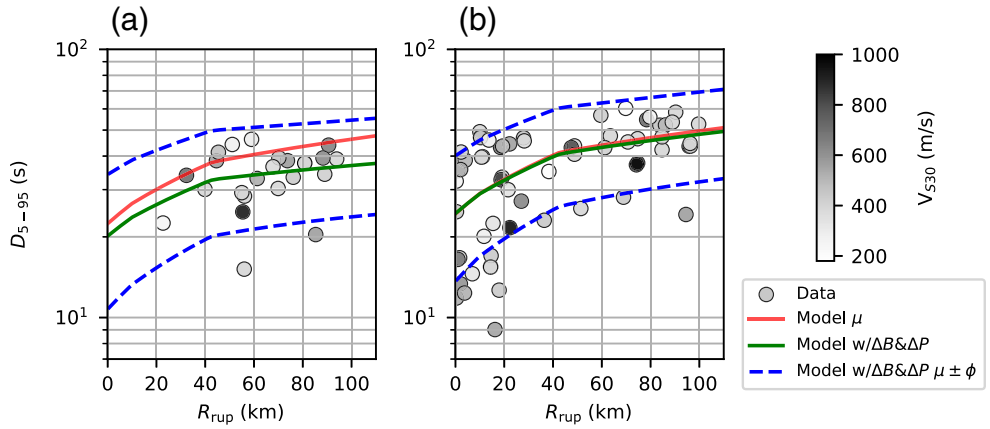

Figure 21. Comparison of the D_{5-95} model with data from the two largest earthquakes of the 2023 Türkiye sequence. The "model μ" curves show the global median. The "model $w/\Delta B$ and ΔP" curves include the event-specific source and path terms. The $\mu \pm \phi$ curves show the range of the within-event standard deviation (for known ΔP and ΔB). (a) M 7.7 Elbistan earthquake ($\Delta B = 0.887$ and $\Delta P = 0.668$). (b) M 7.8 Pazarcik earthquake ($\Delta B = 1.004$ and $\Delta P = 0.931$). The model is shown for $V_{S30} = 400$ m/s. The color version of this figure is available only in the electronic edition.

In the center of the data range, the proposed duration model leads to similar estimates of the median duration as given by current models. The aleatory variability for the D_{5-95} is also similar to the current models in the center of the data range. The use of a power-normal transformation in the proposed model leads to an aleatory variability that depends on the amplitude of duration. Compared with the commonly used lognormal distribution, the proposed duration model has reduced aleatory variability for large values of the median duration (e.g., large magnitudes or large distances) and increased aleatory variability for small values of the median duration (e.g., small magnitude earthquakes at short distances).

A key feature of the proposed duration model is an improved statistical model for the aleatory variability of the ergodic duration model. In particular, the inclusion of a random effect for the path term avoids mapping path effects into event terms. The statistical form also provides the framework for developing region-specific duration models to capture the regional changes in the scattering. This framework is also well suited for moving to nonergodic duration models in the future.

Most duration models use the D_{5-75} or D_{5-95} metrics. The proposed duration model can be used to compute the D_{5-X} duration for any value of X ranging from 10 to 95. This provides a more complete description of the evolution of the amplitude of the shaking strength with time.

The largest contribution to the median in an additive functional form model comes first from the distance scaling and then from the magnitude. Many geotechnical engineering applications that depend on the shaking duration adopt magnitude as a proxy for duration effects, which is reasonable for short distances, but the distance scaling could be more significant than the magnitude scaling for large distances.

The starting time the of the D_{5-X} duration window can be sensitive to the P-wave amplitude. For example, the duration can be lengthened because the 5% of normalized I_A may be reached earlier than the first S-wave arrivals if the P waves have large amplitudes. This effect could be especially significant at large rupture distances with large S-P times. Similarly, the ending times for the 95% I_A can be sensitive to the amplitudes of surface waves or the inclusion of significant ground motion from aftershocks that can lengthen the time to reach 95% of the I_A. Because our duration model includes a more complete description of the evolution of the normalized I_A ($D_5 - X$ for a range of X values), our duration model can be used to compute other duration intervals, such as D_{20-80}, that would be less affected by these edge effects on the signal windowing.

DATA AND RESOURCES

Additional details of the 3D simulations and the EXSIM simulations are given in the supplemental material. The data sets used in this study are given in two files in the supplemental material. The duration data set for D_{5-75} used for the regression is given in the "metadata_and_d575.csv" file. The duration data set for D_{5-X} used for the interduration model is given in the "d5x_dataset.csv" file.

DECLARATION OF COMPETING INTERESTS

The authors acknowledge that there are no conflicts of interest recorded.

ACKNOWLEDGMENTS

The authors want to acknowledge Norman Abrahamson's research group for all the contributions to the development of this article during the weekly meetings, especially; Irene Liou, Maxime Lacour, Franklin Olaya, and Karen Sung. Also, we want to acknowledge the three reviewers of this article. Their thoughtful comments aided in including several improvements in our work.

REFERENCES

Abrahamson, N., W. Silva, and R. Kamai (2014). Summary of the ASK14 ground motion relation for active crustal regions, *Earthq. Spectra* **30,** no. 3, 1025–1055.

Afshari, K., and J. Stewart (2016). Physically parameterized prediction equations for significant duration in active crustal regions, *Earthq. Spectra* **32,** no. 4, 2057–2081.

Ancheta, T., R. Darragh, J. Stewart, E. Seyhan, W. Silva, B. Chiou, K. Wooddell, R. Graves, A. Kottke, D. M. Boore, *et al.* (2014). NGA-West2 database, *Earthq. Spectra* **30,** no. 3, 989–1005.

Arias, A. (1970). A measure of earthquake intensity, in *Seismic Design for Nuclear Power Plant*, R. J. Hansen, MIT Press, Cambridge, Massachusetts, 438–483.

Bahrampouri, M., A. Rodriguez-Marek, and R. Green (2021). Ground motion prediction equations for significant duration using the KiK-net database, *Earthq. Spectra* **37,** no. 2, 903–920.

Bommer, J., P. Stafford, and J. Alarcón (2021). Empirical equations for the prediction of the significant, bracketed, and uniform duration of earthquake ground motion, *Bull. Seismol. Soc. Am.* **99,** no. 6, 3217–3233.

Boore, D. (2009). Comparing stochastic point-source and finite-source ground-motion simulations: SMSIM and EXSIM, *Bull. Seismol. Soc. Am.* **99,** no. 6, 3202–3216.

Boore, D., and E. Thompson (2014). Path durations for use in the stochastic-method simulation of ground motions, *Bull. Seismol. Soc. Am.* **104,** no. 5, 2541–2552.

Bora, S. S., F. Scherbaum, N. M. Kuehn, and P. J. Stafford (2014). Fourier spectral- and duration models for the generation of response spectra adjustable to different source-, propagation-, and site conditions, *Bull. Earthq. Eng.* **12,** 467–493.

Bray, J., and F. Olaya (2022). Evaluating the effects of liquefaction, Submitted to the *J. Geotech. Geoenviron. Eng.*, ASCE.

Bray, J., and T. Travasarou (2007). Simplified procedure for estimating earthquake-induced deviatoric slope displacements, *J. Geotech. Geoenviron. Eng.* **144,** no. 3, 530–533.

Cetin, K. O, M. Ilgac, G. Can, and E. Cakir (2023). Preliminary reconnaissance report on the February 6, 2023, Pazarcik Mw=7.7 and Elbistan Mw=7.6, Kahramanmaras-Turkey earthquakes, *Middle East Technical University Rept. No: METU/EERC 2023-01*, doi: 10.13140/RG.2.2.15569.61283/1.

Herrmann, R. (1985). An extension of random vibration theory estimate of strong ground motion to large distances, *Bull. Seismol. Soc. Am.* **75,** no. 5, 1447–1453.

Idriss, I., and R. Boulanger (2008). *Soil Liquefaction During Earthquakes*, Earthquake Engineering Research Institute, Oakland, California.

Kempton, J. S. (2006). Prediction equations for significant duration of earthquake ground motions considering site and near-source effects, *Earthq. Spectra* **22,** no. 4, 985–1013.

Leonard, M. (2010). Earthquake fault scaling: Self-consistent relating of rupture length, width, average displacement, and moment release, *Bull. Seismol. Soc. Am.* **100,** no. 5, 1971–1988.

Motazedian, D., and G. Atkinson (2005). Stochastic finite-fault modeling based on a dynamic corner frequency, *Bull. Seismol. Soc. Am.* **95,** no. 3, 995–1010.

Petersson, N., and B. Sjögreen (2012). Stable and efficient modeling of anelastic attenuation in seismic wave propagation, *Comm. Comput. Phys.* **12,** no. 1, 193–225.

Petersson, N., and B. Sjögreen (2015). Wave propagation in anisotropic elastic materials and curvilinear coordinates using a summation-by-parts finite difference method, *Comm. Comput. Phys.* **299,** 820–841.

Rathje, E., and A. Kottke (2008). Procedures for random vibration theory based seismic site response analyses, *Technical Rept. Geotechnical Engineering Rept. GR08-09*, Geotechnical Engineering Center, Department of Civil, Architectural, and Environmental Engineering, The University of Texas, Texas, Austin, available at https://www.nrc.gov/docs/ML0806/ML080650274.pdf (last accessed October 2023).

Salvatier, J., T. V. Wiecki, and C. Fonnesbeck (2016). Probabilistic programming in Python using PyMC3, *PeerJ Comput. Sci.* **2,** e55, doi: 10.48550/arXiv.1507.08050.

Seed, H. (1975). Representation of irregular stress time histories by equivalent uniform stress series in liquefaction analyses, *Earthquake engineering research center–Report number EERC 75-29*, Pacific Engineering and Analysis, available at https://pdfcoffee.com/eerc-75-29-pdf-free.html (last accessed October 2023).

Silva, W., N. Abrahamson, G. Toro, and C. Constantino (1996). Description and validation of the stochastic ground motion model, *Technical Report*, Pacific Engineering and Analysis, available at https://www.nrc.gov/docs/ML0428/ML042800294.pdf (last accessed October 2023).

Sjögreen, B., and N. Petersson (2012). A fourth order accurate finite difference scheme for the elastic wave equation in second order formulation, *J. Sci. Comput.* **52,** no. 1, 17–48.

Wells, D., and K. Coppersmith (1994). New empirical relationships among magnitude, rupture length, rupture width, rupture area, and surface displacement, *Bull. Seismol. Soc. Am.* **84,** no. 4, 974–1002.

Manuscript received 16 June 2023
Published online 18 October 2023